Superconducting phase boundary of aperiodic networks in a magnetic field

A. Behrooz
Department of Physics, University of Pennsylvania, Philadelphia, Pennsylvania 19104

M. J. Burns
Department of Physics, University of Pennsylvania, Philadelphia, Pennsylvania 19104 and Division of Applied Sciences and Department of Physics, Harvard University, Cambridge, Massachusetts 02138

D. Levine
Department of Physics, University of Pennsylvania, Philadelphia, Pennsylvania 19104 and Institute of Theoretical Physics, University of California, Santa Barbara, California 93106

B. Whitehead
National Research and Resource Facility for Submicron Structures, Cornell University, Ithaca, New York 14853

P. M. Chaikin
Department of Physics, University of Pennsylvania, Philadelphia, Pennsylvania 19104 and Exxon Research and Engineering Co., Annandale, New Jersey 08801

(Received 19 January 1987)

We have used electron-beam lithography to fabricate superconducting "wire" arrays in a variety of patterns ranging from periodic to random and including the intermediate quasicrystalline and incommensurate configurations. Sweeping an applied magnetic field while observing the critical temperature reveals which fields are favorable or commensurate with the pattern. We find sharp dips in the $T_c(H)$ curve for periodic, incommensurate (quasiperiodic), and quasicrystalline arrays reflecting a lock-in of the flux lattice with the underlying network. We find no similar fine structure for random arrays. This allows us to generalize the concept of commensurability to nonperiodic structures.

I. INTRODUCTION

In the superconducting state the order parameter exhibits long-range phase coherence. The fact that the order parameter must be single valued leads to fluxoid quantization; the appropriate sum of the magnetic flux through any loop and the current circulating the loop must add to an integral number of flux quanta. The first experimental demonstration of this macroscopic quantum effect was done in a ~ 1-μm-diam cylinder by Little and Parks in 1963.[1] The critical temperature was periodic as a function of magnetic field (at the normal-superconducting phase boundary) with period $\Delta H = \Phi_0 / A$ ($\Phi_0 = hc/2e$ being the flux quantum and A the area enclosed by the cylinder). Twenty years later Pannetier *et al.*[2] experimented with superconducting periodic networks. They found the phase boundary to have major structure at $H = nH_0$, $H_0 \equiv \Phi_0 / A$ (n an integer, A the area of an elementary tile or unit cell), similar to the single-loop experiment. Additionally, the phase boundary showed fine structure at fields $H = (n/m)H_0$ (n,m integers), rational fractions of a flux quantum per elementary tile, corresponding to the formation of a commensurate flux superlattice on the underlying pattern. Thus it was shown that the long-range coherence of the superconductor makes it an excellent probe for studying the commensurate configurations of a network.

The main idea of the present work was to perform flux-quantization experiments on networks in which order was a tunable variable. Of great interest was the quasicrystalline state[3] which is often viewed as intermediate between disordered and periodic. It is a nonperiodic tiling of space using a finite number of inequivalent tiles which are quasiperiodically repeated. Thus, like an ordered state it can be specified by a few parameters, and like a disordered state it is not periodic. Intermediate between quasicrystalline and random is an incommensurate structure, made by the superposition of two or more irrationally related periodic structures. It is quasiperiodic but it has an infinite number of inequivalent tiles. In the sequence of decreasing order, our samples consisted of crystalline, quasicrystalline, incommensurate, and random structures.

In the next section of this paper we will review what has been learned about flux quantization in periodic networks, since we will draw from this insight into more complex patterns. We will also introduce a simple model of the energetics involved in arranging the fluxoids in particular configurations in the cells of the underlying pattern. In Sec. III we describe the experimental procedures and in Sec. IV we discuss our results. We will conclude that the major structure in the critical-temperature–versus–critical-field phase boundary, which occurred at fields given by nH_0 in the periodic case, is replaced by a power series $\Delta^n H_0$ in the quasicrystalline case

(where Δ is a number characterizing the quasiperiodicity of the network). The fine structure, given by $(n/m)H_0$ for the periodic case, is replaced by $(n+m\Delta)H_0$. From these results we conclude that the magnetic field can form "commensurate" flux lattices on quasiperiodic networks. We then introduce a definition for commensurability which applies to both periodic and quasiperiodic systems.

II. FLUX QUANTIZATION ON PERIODIC ARRAYS

The superconducting order parameter must be single valued; thus the phase integral around any closed loop must be 2π times an integer. In the presence of a magnetic field this quantization condition becomes[1]

$$\oint \nabla\Phi\cdot dl=\frac{4\pi}{c\Phi_0}\oint \lambda^2\mathbf{J}\cdot dl+\frac{2\pi}{\Phi_0}\oint \mathbf{A}\cdot dl=2\pi n \ , \quad (1)$$

where Φ_0 is the flux quantum $hc/2e=2.07\times10^{-7}$ gauss cm^2, and λ is the penetration depth. The integral over the vector potential is just the magnetic flux through the loop and the phase integral (known as the fluxoid) must always be quantized. Consider a single loop. If the magnetic field through the loop is exactly an integral number of flux quanta, Eq. (1) is satisfied with no currents circulating the loop. Then the additional kinetic energy ($E\propto J^2$) is a minimum and the transition temperature is a maximum. In the case of a single loop

$$T_c(0)-T_c(H)\sim E\approx(\xi/a)^2(n-\Phi/\Phi_0)^2 \ ,$$

where n is an integer giving the number of fluxoids in the loop, ξ the superconducting coherence length, a the radius of the loop, and Φ the flux through the loop. The phase boundary is obtained by choosing n such that the energy is minimized, as was shown in the work of Little and Parks.[1]

The problem becomes considerably more complex when we deal with a periodic network,[4-7] because the quantization condition has to be met around every closed path. To calculate the phase boundary the linearized Ginzburg-Landau (GL) equations have to be solved under the constraint of current conservation at each node of the network. The resulting equation relates the order parameter at node i (denoted by Δ_i) to the order parameter at all of its nearest-neighbor nodes (Δ_j):

$$-\Delta_i\sum_j\cot(\Theta_{ij})+\sum_j\Delta_j e^{i\gamma_{ij}}/\sin(\Theta_{ij})=0 \ , \quad (2)$$

where $\Theta_{ij}=l_{ij}/\xi_s$ is the distance between nodes divided by the coherence length and $\gamma_{ij}=\int_i^j(2e/\hbar c)\,\mathbf{A}\cdot dl$. For networks where all links are of equal length, the above equation reduces to that of a tight-binding electron on a similar lattice in a magnetic field, with the energy given by $E=\cos(l/\xi_s)$.

The network equations are not particularly illuminating and due to their complexity require computer solutions. To understand qualitatively what we might expect, it is convenient to imagine the limit where the wires which make up the network have a diameter which is much larger than the penetration depth, and much smaller than the unit-cell dimension. In the center of the wires the current is then negligible and the flux through any closed path is quantized. In this limit the currents flowing at the surfaces of wires must produce a magnetic field which makes up the difference between the applied field and an integral number of flux quanta. The "rules" for this simplified model calculation are then current conservation at each node, and an average field for the entire network which is equal to the applied field. For example, an applied field $H<\Phi_0/A$ (A is the area of a unit cell) would correspond to a fraction f of the unit cells having a penetrating flux quantum and $1-f$ having zero flux, with $f\Phi_0/A=H$. The currents required for this arrangement can be calculated, and with that the kinetic energy and ΔT_c are known. (There is an additional energy from the induced currents interacting with the applied field which we have neglected.[4] It does not depend on the particular arrangement of the flux lines, which is our major concern.)

How does this model relate to the actual experimental situation? In the experiments λ is much larger than the width of the wires and the screening currents are very small. These currents produce magnetic fields which are perturbations on the applied field and are neglected in most treatments. [The most difficult problem to solve would be the self-consistent treatment of Eq. (1) with non-negligible magnetic fields generated by the currents and non vanishing λ.] In our model calculation λ is zero, but the field produced by and proportional to the currents is sufficient to augment the magnetic field such that Eq. (1) is satisfied completely by the magnetic flux and we have flux quantization rather than fluxoid quantization. The net result is that the currents in our model, though much larger than the currents in the experimental situation, are nevertheless proportional to them. Thus the kinetic energies calculated from our model will be in the correct ratios and the T_c shifts will be qualitatively correct. (What prevents an exact correspondence to the experiment is the presence of amplitude variations of the order parameter in the GL equations. The present model only concerns phase variations.) The main advantage of the simpler model is the ability to evaluate the energies corresponding to different configurations of flux quanta on the network. In translating back to the experimental situation, we associate a tile with n piercing flux quanta in our model with a tile containing n fluxoids in the experiment.

If we ignore correlations between occupied and unoccupied tiles, we can proceed to calculate the currents. In an applied field $H=\Phi/A=f\Phi_0/A$, f tiles require a current proportional to $\Phi_0(1-f)$, while $1-f$ tiles require a current proportional to $\Phi_0 f$. In this situation all tiles will satisfy flux quantization. The average current is zero (as it must be to ensure the average field as the applied field); however, the average squared current circulating around each tile is

$$f(1-f)^2\Phi_0^2+(1-f)f^2\Phi_0^2=f(1-f)\Phi_0^2=\Phi(\Phi_0-\Phi)$$

for $f<1$.

The above arguments are easily generalized to any field

and we have $\Delta T_c \sim (\Phi/\Phi_0 - m)(m+1-\Phi/\Phi_0)$, where m is an integer. For an infinite network, ΔT_c is zero for $H = n\Phi_0/A$ ($n=0,1,2,\ldots$), but ΔT_c increases linearly close to these fields rather than quadratically (as for the single-loop problem). Thus the periodicity of the phase boundary is again in terms of integral number of flux quanta per tile, but now we have cusps instead of parabolas at each minimum.

There are additional structures at nonintegral flux quanta per tile which result from the correlations which we neglected above. The most straightforward example is the case where $H = \Phi_0/2A$. If we randomly fill half of the tiles the result is $\langle J^2 \rangle = \frac{1}{32}$. However, if we correlate the tiles with flux quanta so that they only share edges with tiles without flux (as a checkerboard for the square lattice), then the kinetic energy is decreased to $\langle J^2 \rangle = \frac{1}{64}$. Similarly, there is a favorable correlated arrangement of the flux quanta for any rational fraction of a flux quantum per tile.[2,8,9] This is equivalent to having a flux lattice commensurate with the underlying periodic pattern.

The lessons from flux quantization in periodic arrays is then that the large-scale structure and periodicity of the phase boundary are related to the size and uniformity of the individual tiles in the array. A flux of $n\Phi_0$ piercing a tile is equivalent to the zero-field state, since no screening currents are induced. The fine structure at any rational fraction of a flux quantum per tile is related to the arrangement of the flux quanta (or fluxoids in the experimental situation) on the underlying network with the flux (fluxoid) lattice locking into commensurate coverages, thereby reducing the kinetic energy.

What would be the nature of the $T_c(H)$ phase boundary for incommensurate or quasicrystalline networks? For the quasicrystalline patterns we have two irrationally related tile areas, which will preclude the field from satisfying flux quantization around all tiles of the network for any field. This should dramatically affect the large-scale structure. Any fine-scale structure in the phase boundary of the quasicrystalline or incommensurate patterns will signify a locking in of the field which has found a way to be "commensurate" with the network.

III. EXPERIMENTAL DETAILS

The samples were fabricated at the National Research and Resource Facility for Submicron Structures at Cornell University. Micrographs of four of the patterns we report on, along with their optical diffraction patterns, are shown in Fig. 1. Three of the patterns are one dimensional, i.e., they are made of parallel lines in the x direction, crossed by lines in the γ direction that are in a Fibonacci[3] sequence, in a random Fibonacci (RF) sequence, or in a sequence of two incommensurate periods (TIP).

The Fibonacci pattern shown in Fig. 1(a) consists of N_L tiles of area A_L and N_S tiles of area A_S, where $N_L/N_s = \tau$, $A_L/A_S = \tau$, and the golden mean is given by $\tau = (1+\sqrt{5})/2 = 1.618\ldots$. The placement of "longs" and "shorts" is determined by a Fibonacci sequence. (The algorithm we use is $y_n = n + 1/\tau[n/\tau]$, the square brackets denoting that we take the largest integer part, n is an integer, and x_n determines the distance of the nth line from the origin.) The tile dimensions were on the order of a few micrometers, conveniently allowing for diffraction of visible light. Next to the optical micrograph of each pattern, we show the optical transform obtained simply by diffraction of a He-Ne laser beam. For the Fi-

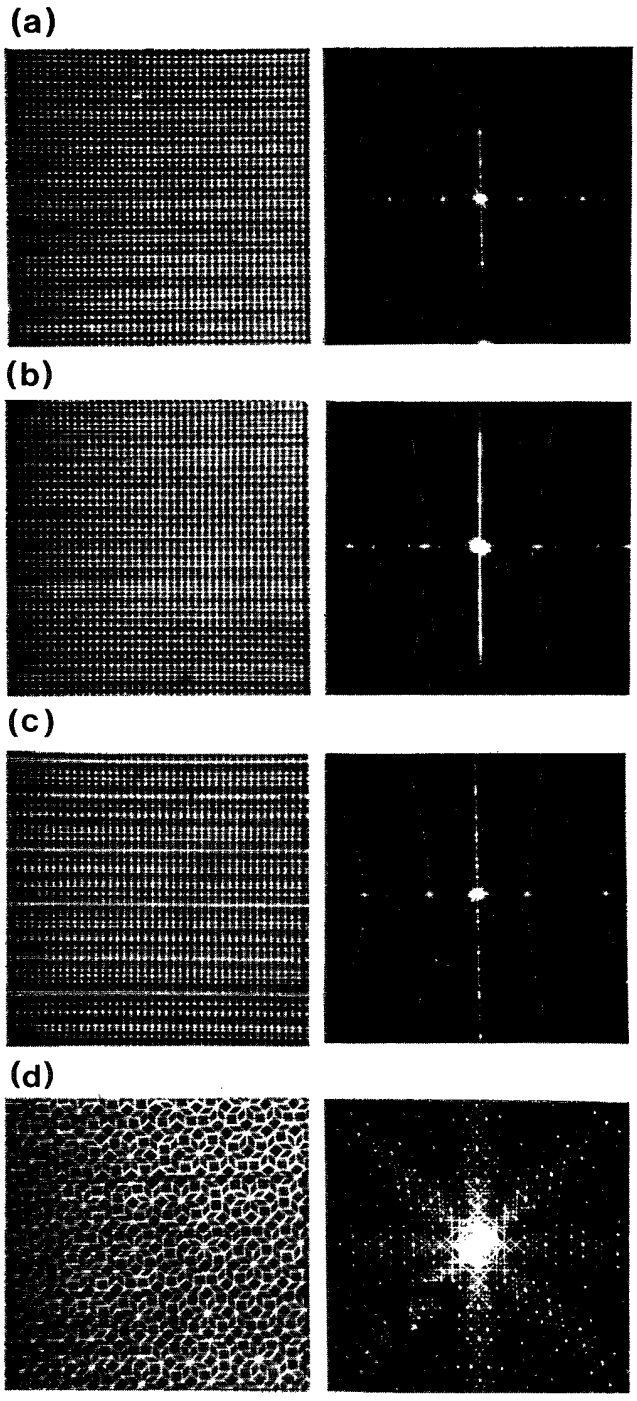

FIG. 1. Optical micrographs and corresponding diffraction patterns of (a) Fibonacci, (b) random Fibonacci, (c) two incommensurate periods, and (d) eight-fold symmetric "Penrose" networks.

bonacci pattern the optical transform (Fourier spectrum) consists of a dense set of points at $(n+m\tau)$ reflecting the quasiperiodicity,[3] i.e., an infinite set of frequencies related to the two lengths 1 and τ. In the Fibonacci pattern both the ratio of the areas and the quasiperiodicity are characterized by the number τ. In order to distinguish the effects of the quasiperiodicity from that of the irrational area ratio we made the RF pattern shown in Fig. 1(b). As in the Fibonacci pattern the ratio of the areas is τ and there are τ times as many large as small tiles. However, the tiles are randomly arranged. The optical transform reflects this in showing diffuse scattering instead of distinct Bragg peaks. Note, however, that the scattering intensity $S(q)$ is not a monotonic function of wave vector q. There are strong peaks, as expected from the calculation of Hendricks and Teller.[10]

The TIP pattern, shown in Fig. 1(c), is made by putting down a set of periodically spaced lines with distance $a_S \approx 3.24$ μm and on top of that another set of lines with the distance $a_L = \tau a_S \approx 5.24$ μm. In this pattern we have a distribution of hole sizes from zero up to the largest hole, given by the smaller spacing a_S times the periodicity in the y direction. The quasiperiodicity of this pattern is evident from the Bragg peaks in the optical transform at $2\pi n/a_L$ and $2\pi m/a_S = 2\pi(m\tau)/a_L$; there are only two frequencies in the spectrum.

In addition to our one-dimensional patterns we have made a two-dimensional quasicrystal.[3] It is shown in Fig. 1(d) and is the eight-fold symmetric version of a Penrose tile. (We were not able to make a Penrose pattern because the microfabrication apparatus cannot draw links at an angle of 72°.) It is made up of two elementary tiles, a fat and a skinny one, with a relative area ratio of $\Sigma = \sqrt{2}$. Unlike the Penrose tiling, there are more skinny tiles than fat ones by the ratio Σ. The quasiperiodicity is characterized by the number of $\sigma = 1+\sqrt{2}$. The pattern is generated by an inflation scheme[3] with each inflation changing characteristic distances by σ. The Fourier spectrum is similar to the Fibonacci spectrum in that it is given by a dense set of points, for example $n+m\sigma$ along any of the eightfold axes.

The patterns were generated by a Cambridge EBMF-2-150 electron-beam microfabricator according to a computer code. The patterns were written into a multilayer resist which was spun onto a silicon wafer. After liftoff of the exposed resist we were left with a mask onto which we evaporated pure aluminum. After liftoff of the mask, we had networks made of typically 3000-Å wide and 500-Å-high wires of aluminum supported on a silicon wafer. Our "one-dimensional" patterns had 400×400 lines. The periodic lines in the x direction were separated by 2 μm, and the total sample area was 800 μm^2. Thus the Fibonacci and random Fibonacci patterns had tiles of areas $A_L = 4.7$ μm^2 and $A_S = 2.9$ μm^2. The eight-fold "Penrose" pattern had about 20 000 elementary tiles, and the area of the large elementary tile was 7.6 μm^2.

The resistivity of the aluminum at 4 K was ~ 1.0 $\mu\Omega$ cm as inferred from four-probe resistance measurements. The superconducting coherence length was $\xi(0) = 0.855(\xi_0 l) \sim 0.20$ μm, where we use $\xi_0 = 1.6$ μm as the coherence length for bulk Al and $l \sim 400$ Å for the mean free path. The typical resistive transition was ~ 2 mK wide and this width did not change appreciably with fields up to 30 G. The sample, a resistive heater, and a thermometer were mounted on a copper platform of low thermal mass, which, in turn, was connected to a ^{3}He pot via brass standoffs. The $T_c(H)$ phase boundary was obtained by using a feedback loop to keep the sample at a constant resistance (typically in the middle of the superconducting transition) while sweeping the magnetic field. At constant field the temperature control thus achieved was better than 50 μK. While sweeping the field the critical temperature could then be continuously recorded. Typical data shown are the average of 36 field sweeps.

IV. EXPERIMENTAL RESULTS AND DISCUSSION

One of the aims of the present study was to see whether the quasiperiodic or quasicrystalline network could readily be distinguished from a random pattern in the flux-quantization experiment. The three samples basic to this question are the Fibonacci, RF, and TIP patterns. Their phase boundaries, $T_c(H)$, are shown in Figs. 2(a), 3, and 6. The answer is immediately apparent. The fine structure which indicates a locking of the flux arrangement with the network, i.e., "commensurability," is only present in the Fibonacci and TIP patterns which are quasiperiodic and hence have long-range order. Thus there is a sense of commensurability with these structures. As might be expected, the RF pattern has the same overall large-scale behavior as the Fibonacci, reflecting the same area ratio of the elementary tiles, but does not show fine structure because the tiles are randomly arranged and the dips are parabolic rather than "cusplike." Note that none of the $T_c(H)$ curves are periodic and that they do not return to $\delta T_c = 0$ (except perhaps asymptotically as $H \to \infty$); both of these properties are a consequence of the irrational areas.

In order to get a better understanding of the Fibonacci and RF phase boundaries, it is instructive to apply the models developed in Sec. II. The ratio of the tile areas in the Fibonacci and RF patterns is irrational. This means that flux quantization cannot occur in the absence of screening currents, except at infinite field strength. For any given field, currents must be set up to add to the applied field in the small (or large) tiles and to subtract from the applied field in the large (or small) tiles. There are fields where these currents are minimized. At these fields there are N_L (N_S) flux quanta in the large (small) tiles and the ratio N_L/N_S approximates the area ratio τ. The best successive approximates to τ are given by F_{n+1}/F_n, where F_n is the nth Fibonacci number. The Fibonacci sequence is generated by $F_{n+1} = F_n + F_{n-1}$; starting with $F_0 = 0$ and $F_1 = 1$, we have the sequence 0,1,1,2,3,5,8, ... Thus the minima for $\langle J^2 \rangle$ occur at field strengths where we have $(N_L, N_S) = (1,1)$, (2,1), (3,2), (5.3), (8,5), . . . , where the ratios N_L/N_S are just the successive rational approximates to τ. Since these ratios are successively better approximates to τ, the corresponding dips should asymptotically approach the zero-field T_c. The fields at which we should then expect the major dips are

$$H=(N_L n_L+N_S n_S)\Phi_0/(n_L A_L+n_S A_S)$$
$$=(\tau N_L+N_S)\Phi_0/(1+\tau^2)A_S$$
$$=(\tau F_{n+1}+F_n)\phi_0/(1+\tau^2)A_S=\tau^{n-1}H_0$$

where $H_0=\tau^2\phi_0/(1+\tau^2)A_S$, $n=1,2,3,\ldots$, n_S is the number of small tiles, $n_L=\tau n_S$ is the number of large tiles, A_S is the area of a small tile and $A_L=\tau A_S$ is the area of the large tile, and where we have used the relation $\tau^{n+1}=F_n+\tau F_{n+1}$. Since the quasiperiodicity of the pattern did not come into the above argument we expect that both the Fibonacci and the RF patterns will have a series of dips in a power series of τ. The phase boundaries $T_c(H)$ for the Fibonacci and RF patterns are shown in Figs. 2(a) and 3. A parabolic background related to the critical field of the finite-size wires has been subtracted. With $1,\tau,\tau^2,\ldots$, we have marked the fields at which we have, respectively, $(N_L,N_S)=(1,1)$, $(2,1)$, $(3,2)$, ... The data show the overall similarity between the Fibonacci and RF patterns. There is, however, a fundamental difference between the two; while the Fibonacci pattern shows abundant cusplike fine structure, the RF curve is comparatively smooth. This signifies the importance of the quasiperiodic long-range order to the preferential "commensurate" ordering of the fluxoid lattice.

As a first attempt at a quantitative calculation of $T_c(H)$ for the Fibonacci and RFIB patterns, we treated the case of two tiles with an area ratio τ. This is somewhat analogous to treating a single loop for the periodic array. The two-tile problem can be solved exactly using the network equations [Eq. (2)]. The result of this calculation for the upper critical temperature is shown in Fig. 4. All the structures can be identified by how many flux quanta or fluxoids are piercing the large and small tiles (N_L,N_S). The largest dips occur at fields where N_L and N_S are successive Fibonacci numbers, which give the best rational approximates to the area ratio. Since $F_{n+1}=F_n+F_{n-1}$, the dips occur at successive Fibonacci numbers. Starting with $F_0=0$ and $F_1=1$, the first dip at (1,0) corresponds to F_2, the dip at (1,1) to F_3, etc. (see Fig. 4). In the two-tile case

$$H=\Phi_0(N_L+N_S)/(A_L+A_S)=H_0F_n$$

rather than

$$H=\Phi_0(\tau N_L+N_s)/(\tau A_L+A_S)=H_0\tau^{n-1}$$

as for the Fibonacci and RF patterns.

To do a better job of calculating the phase boundary, we have solved the GL equations on a 23×23 grid of the Fibonacci pattern.[11] (The calculation has been greatly simplified by using the periodicity in the x direction to introduce a discretely variable Floquet factor.) The result is shown in Fig. 2(b) and should be compared with the Fibonacci pattern [Fig. 2(a)]. There is agreement in both the fine and large-scale structure. An additional feature which appears in the calculation is a quasimirror symmetry about the points $(\tau^n+\tau^{n+1})/2$ which extends from 0 to $\tau^n+\tau^{n+1}$.[12] This feature is also evident in the calculation of the two irrationally related tiles, but in this case

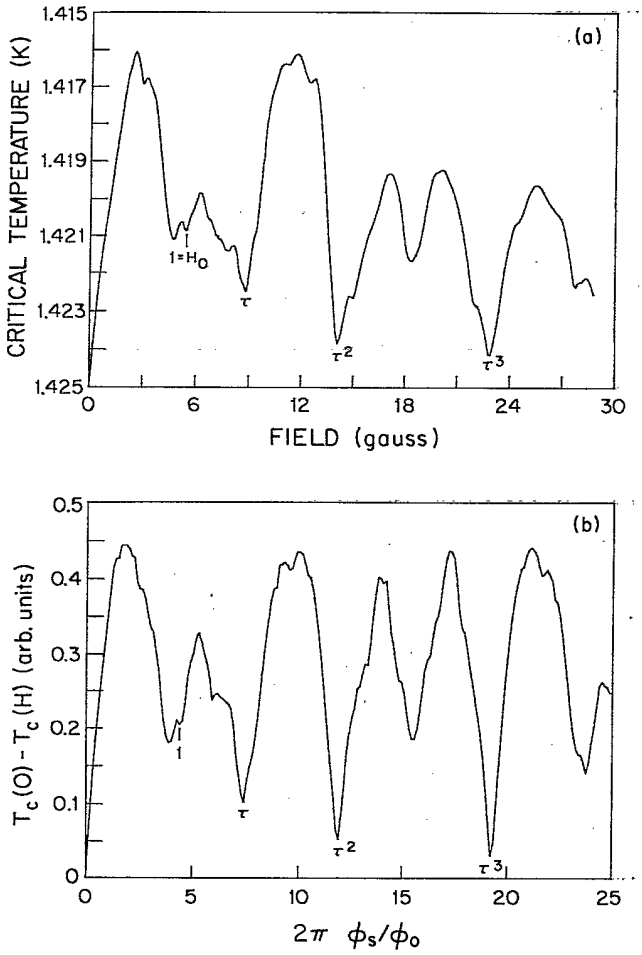

FIG. 2. Superconducting transition temperature vs magnetic field for the Fibonacci pattern. (a) Experimental data after subtraction of a parabolic background. (b) Calculated $T_c(H)$ from linearized Ginzburg-Landau theory. Φ_S is the flux through a small tile.

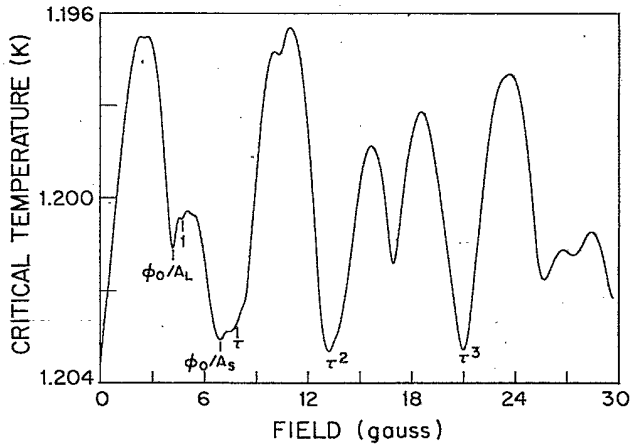

FIG. 3. $T_c(H)$ for the random Fibonacci pattern, after subtraction of a parabolic background. Φ_0/A_L (Φ_0/A_S) is the field that corresponds to one flux quantum in the large (small) tiles.

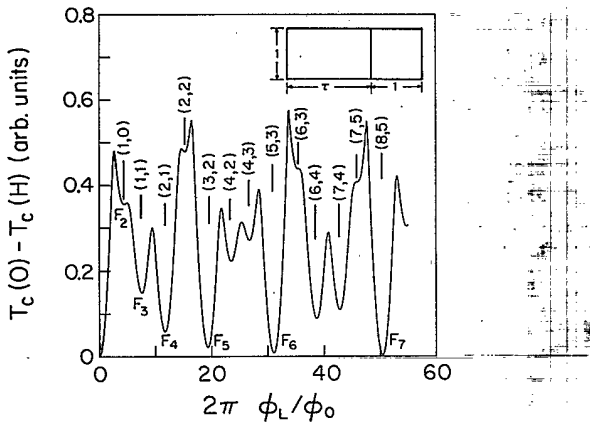

FIG. 4. Calculated $T_c(H)$ for the two-tile network shown in the inset using the linearized Ginzburg-Landau equations. All structure seen is labeled by the number of flux quanta (N_L,N_S) piercing the large and small tiles. Major structure occurs at successive Fibonacci numbers. Φ_L is the flux through the large tile.

the symmetry is about the midpoint between two Fibonacci numbers.

A closer look at the phase boundary of the Fibonacci pattern reveals that not all the structure is equivalent; some dips are cusplike while others are more parabolic. Remembering that in the single-loop experiment we saw parabolic dips while in the regular network we had cusps makes it possible to know the origin of the structure seen. Most of the structure is cusplike, e.g., the dips at $1,\tau,\ldots,$ indicating that these are due to coherence effects of the whole pattern. Now consider the dip which is slightly lower in field than the dip identified by 1. Here the field is just large enough to satisfy flux quantization in the large tile ($H=\Phi_0/A_L$). Thus the net current circling the large tiles is zero, while the small tiles have fairly large screening currents. The corresponding dip is parabolic, because this is a single-tile effect. Notice that the structure in the RF pattern is more rounded than in the Fibonacci pattern. The RF pattern due to its randomness does not allow "commensurate" flux patterns, and should only show parabolic dips. The largest structures in the RF boundary at low fields are due to single-tile effects; the dip at Φ_0/A_L occurs when flux quantization is satisfied around the large tiles. Similarly, Φ_0/A_S satisfies flux quantization around the small tiles. RF patterns that were generated with a different random number seed and thus had a different sequence of long tiles and short tiles gave phase boundaries that differed significantly.

Indexing the fine structure for the Fibonacci case is complicated by the periodicity in the x direction. Some of the fine structure is due to quasiperiodicity in the y direction, and some due to the periodicity in the x direction. Identifying the fine structure is much more easily done for the two-dimensional pattern, the eight-fold symmetric tiling. Here the field that corresponds to N_L (N_S) flux quanta in the large (small) tiles is given by

$$H(N_L,N_S)=(\Phi_0/2A_L)(N_L+\sqrt{2}N_S)\ .$$

The area ratio of the tiles in this pattern is $\Sigma=\sqrt{2}$ and there are Σ times as many small tiles as large ones. We expect the major structure to be at field values that correspond to rational approximates to $\sqrt{2}$; $(N_L,N_S)=(1,1)$, (3,2), (7,5), ... If these values are used in the above equation, we get $H=H_0\sigma^n$ $(n=0,1,2,\ldots)$ and H_0 is the field that corresponds to one flux quantum in each elementary tile $[H_0=(1+\sqrt{2})\Phi_0/2A_L]$. The phase boundary for this pattern has been calculated by Nori *et al.*[13] The experimentally obtained phase boundary is shown in Fig. 5. The apparent increase of $T_c(H)$ above $T_c(0)$ for some fields is due to the inadequacy of the quadratic subtraction for a network with some variation in the width of the wires. Note that although we have taken rational approximates to $\sqrt{2}$, the major dips occur in a power series in $\sigma=\sqrt{2}+1$, which is the number characterizing the quasiperiodicity rather than the area ratio. The area ratio and the quasiperiodicity are intimately related in quasicrystals of two or more dimensions. In one dimension they are not; we can replace the long and short tiles in the Fibonacci pattern with two tiles of arbitrary relative area.

The most interesting aspect of the phase boundary is the existence of a considerable amount of sharp cusplike fine structure. From the periodic systems we know that this structure is related to the "rationality" (n/m) of the field and the lock-in of the flux lattice at "commensurate" configurations. What is the generalization of the structures seen at $H=(n/m)H_0$ to the quasicrystalline case? The fine structure as seen in Fig. 5 can be identified by using the quasiperiodicity index σ, such that $H=H_0\,|\,n+m\sigma\,|$. Most of the fine structure seen can be labeled with $|\,n\,|,|\,m\,|\leq 4$. Since any number can be approximated by $n+m\sigma$, or by p/q, we expect that the former is the generalization of the latter for the quasicrystal. However, it is not yet clear how to order the approximates $n+m\sigma$. In the periodic case of p/q the magnitude of the T_c shifts are simply related to the denominator q.

In contrast to all of the other patterns, the quasiperiodic TIP pattern has a continuum of hole sizes, from the

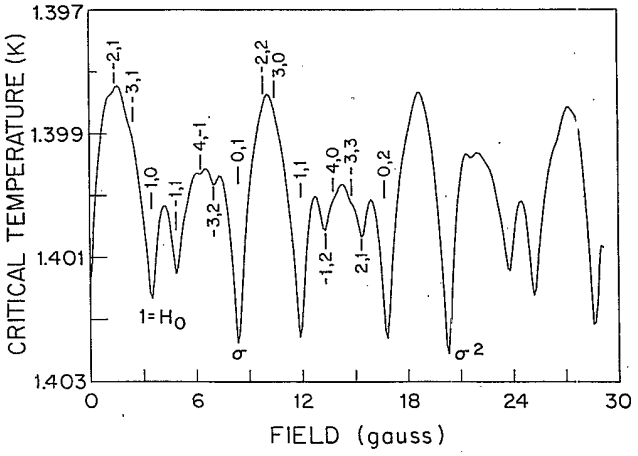

FIG. 5. $T_c(H)$ for the eight-fold symmetric "Penrose" network (after the subtraction of a parabolic background). Numbers n,m indicate the fields $H=H_0\,|\,n+m\sigma\,|$, $\sigma=1+\sqrt{2}$.

largest allowed area down to zero. (The largest area is given by the smaller period in the y direction, 3.24 μm, multiplied by the period in the x direction, 2 μm). Due to this range of tile areas the applied field can never satisfy flux quantization on a major set of tiles, nor can it approximate flux quantization as in the case of the quasicrystals. The phase boundary should then show a sharp rise from zero field (similar to the other samples) and should not show any major structure related to the individual tiles (except for the cutoff due to the largest tiles) and therefore should never approach the zero-field transition temperature. The phase boundary is shown in Fig. 6(a) (a parabolic background has been subtracted). A comparison with the previous phase boundaries shows that the structure is much smaller. However, we see a great amount of cusplike fine structure, indicating that the flux lattice can be "commensurate" with the underlying grid. This is not surprising since the pattern has long-range coherence. A flux lattice can be commensurate with either of the two periods and lose no energy from the other period with which it is incommensurate.

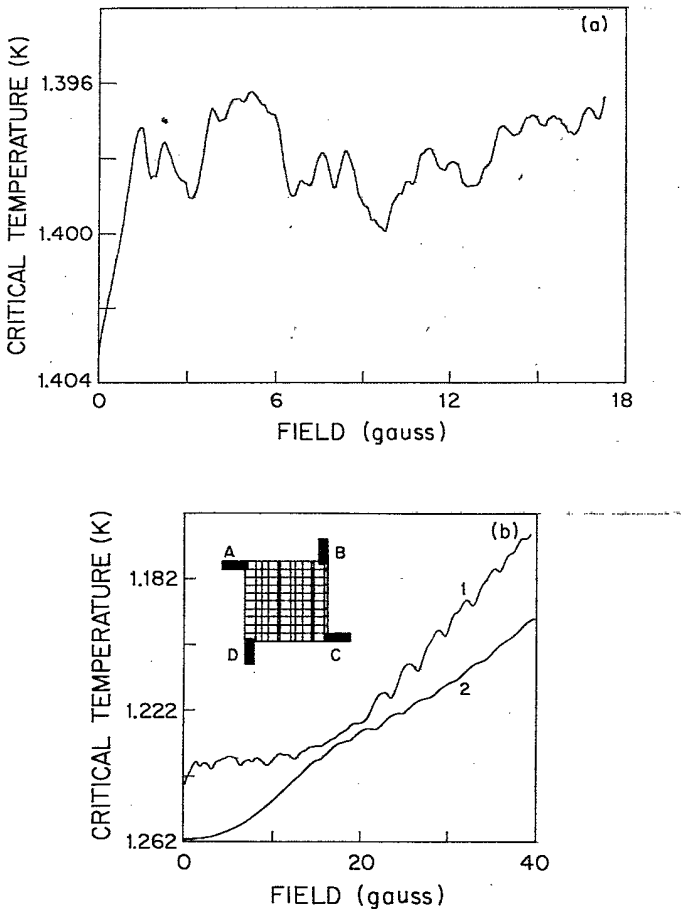

FIG. 6. Inset: Schematic diagram of the two incommensurate periods pattern with four contact leads labeled A, B, C, and D. $T_c(H)$ for this pattern. (a) and curve 1 of (b) correspond to current injection through leads AB and measuring the voltage across CD. Curve 2 of (b) corresponds to current injection through AD and voltage pickup across BC. A parabolic background has been subtracted from curve (a).

Another interesting feature of our experiments is that, in general, for our "one-dimensional" samples we get different results for $T_c(H)$ depending on how we did the measurement. These patterns had four contact leads, each contact touching one corner of the square-shaped sample. Using a pair of neighboring leads for current injection and the other pair for the voltage measurement, there are two different ways of measuring resistance: in one case we mostly probe the periodic grid lines and in the other case the Fibonacci, RF, or TIP lines. (The eight-fold "Penrose" tile is isotropic, and shows the same structure regardless of where on the sample we do the measurement.)

In Fig. 6(b) we have the $T_c(H)$ for the TIP sample. Curve 1 [as well as Fig. 6(a)] corresponds to probing of the periodic lines. We see the fine structure, as mentioned earlier, as well as a set of periodic dips (the period is $\sim$3.2 gauss). The dips correspond to fields $H=n\Phi_0 A$ [n is an integer, $A=a_S(2\ \mu\text{m})$, where 2 μm is the wire spacing in the periodic direction and $a_S=3.24$ μm], which puts an integral number of flux quanta into the largest hole. In this sample the fraction of largest holes to all holes is given by $(\tau-1)/(1+\tau)$. Approximately 24% of all tiles have area A, and when these tiles contain an integer number of flux quanta we see the largest structure in the phase boundary.

Curve 2 corresponds to probing the TIP lines. A look at the TIP micrograph, Fig. 1(c), reveals that while the periodic lines are all of uniform width, the TIP lines come in various sizes. Due to undercutting, two lines written very closely into a multilayer resist will fuse, giving rise to one broad line. In understanding curve 2 it helps to group the TIP lines into "thin" and "thick" lines. Curve 2 can be broken up into two regimes. For fields up to 15 gauss the "thick" lines are shorting out the sample and all we see is their parabolic $T_c(H)$ contribution. (The "thick" lines have a higher T_c and a larger parabolic field dependence than the "thin" lines.) At around 15 gauss we reach the critical field of these lines and we start seeing contributions from the "thin" lines. The oscillations we see for $H>15$ gauss have the same period as the dips in curve 1, and are presumably of the same origin.

We have data on three other "one-dimensional" samples which probe the effects of the incommensurate area ratio and the quasiperiodicity. The first of these is like our Fibonacci pattern, except for the area ratio, which is now equal to $\theta=2$. The generating function we use is $y(N)=a_S N+[N/\tau](a_L-a_S)$, where the square brackets denote taking of the integer part, and a_L, (a_S) are the long (short) spacings in the y direction with $a_L/a_S=\theta$. The quasiperiodicity is still characterized by the irrational number τ. This sample is different from all the others because the ratio of areas is a rational number. Thus the phase boundary has to be periodic. The field that puts two (one) flux quanta into the large (small) tile satisfies flux quantization with no currents circling the wires. The phase boundary thus returns to its zero-field value for $(N_L,N_S)=(2,1)$, (4,2), (6,3), ... In Fig. 7 we show the phase boundary. The major structure is marked with the

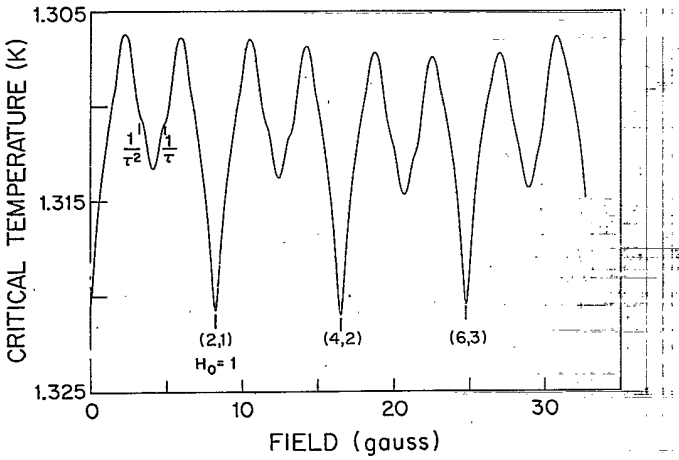

FIG. 7. $T_c(H)$ for a "Fibonacci" pattern with an area ratio of 2. (A parabolic background has been subtracted.) Major structure is labeled by (N_L,N_S), the number of flux quanta piercing large and small tiles. Some of the fine structure related to the quasiperiodicity τ is marked.

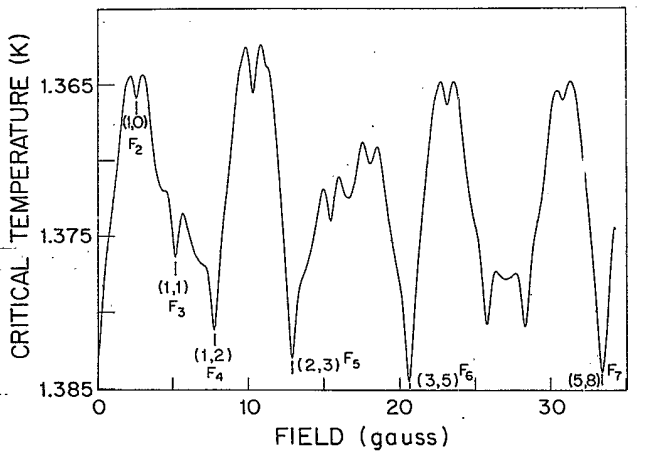

FIG. 9. $T_c(H)$ for a periodic network with a unit cell containing two tiles of area ratio τ. (A parabolic background has been subtracted.) Major structure appears at fields labeled by (N_L,N_S), which are successive Fibonacci numbers.

corresponding (N_L,N_S). Some of the fine structure is related to the quasiperiodicity given by τ. There are dips at H_0/τ and at H_0/τ^2, where we label the field (2,1) with H_0.

The second of these is again like the FIB pattern, except for the area ratio, which is $\theta=(7)^{1/3}$. Figure 8 shows the phase boundary for this sample. There exists a striking resemblance with the data in Fig. 7. Since this θ is very close to the number 2, at low fields $N_L=2N_S$ is a good approximation to θ. Thus, we have the resemblance to the $\theta=2$ sample. However, unlike Fig. 7, Fig. 8 is not periodic. The first three rational approximates to θ are (1/1), (2/1), and (21/11). A GL calculation for a sample with two tiles with the relative area ratio of θ gives some clues as to what happens. We see a series of dips for $N_L=2N_S$ and for $N_L=2N_S-1$ in the interval (2,1) to (21,11). As we increase the field from (2,1) to (21,11), the dips for $N_L=2N_S$, which start out as the largest dips, get smaller, while the dips at $N_L=2N_S-1$ get larger. There is a crossover region halfway between (2,1) and (21,11) at which point $N_L=2N_S-1$ becomes a better approximation to θ than $N_L=2N_S$. Thus as the field increases from (2,1) to (21,11), the dips at $N_L=2N_S-1$ become successively larger while dips at $N_L=2N_S$ become smaller. This gives rise to a quasimirror symmetry about $[(21,11)-(2,1)]/2$ which extends from 0 to (2,1) + (21,11).

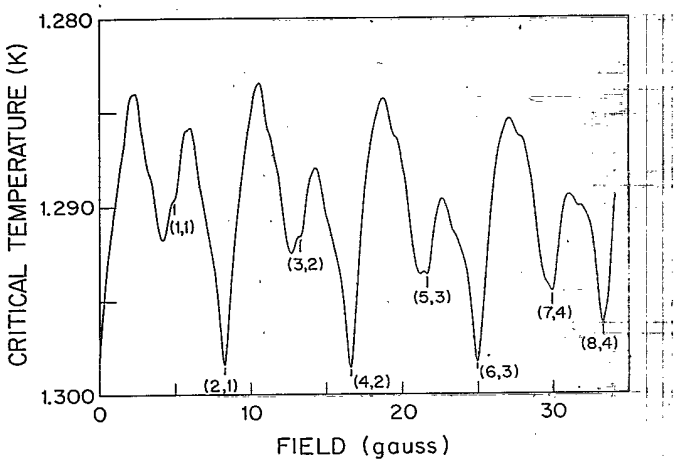

FIG. 8. $T_c(H)$ for a "Fibonacci" pattern with an area ratio of $(7)^{1/3}$. (A parabolic background has been subtracted.) Structure has been labeled by (N_L,N_S), the number of flux quanta piercing large and small tiles.

The third pattern of this study is made by a periodic repetition of a unit that contains a large and a skinny tile that stand in the ratio of τ. In this case the fine structure will be determined by the periodicity in the x and y directions, while the gross structure relates to the ratio τ of the two incommensurate areas. The major dips should correspond to those in the two-tile calculation shown in Fig. 4, but now they are cusplike rather than parabolic. In Fig. 9 the phase boundary of this sample is shown (a parabolic background has been subtracted). The major structure has been marked with the corresponding (N_L,N_S) and Fibonacci number F_n.

V. CONCLUSION

The most interesting finding of our work is that a magnetic field can distinguish between a random and a quasiperiodic structure. The field in the form of a flux lattice locks into "commensurate" states with the underlying quasiperiodic network, similar to epitaxy. Thereby the energy due to screening currents is reduced and the state shows up as a cusplike structure on the $T_c(H)$ phase boundary. We further found that the "commensurate" structures of a quasicrystal can be indexed by $H=H_0(n+m\sigma)$, where σ characterizes the quasiperiodicity, n and m are integers, and H_0 some unit field. No

such "commensurate" states exist on a random array. The question that remains to be answered is how can we tell if a given vortex configuration on a quasicrystal is commensurate? The more general question is when do we call a superlattice arrangement commensurate with the underlying lattice? We propose the following definition: The diffraction pattern of the superlattice should not contain any diffuse scattering, because that would indicate randomness. Then, a superlattice arrangement will be commensurate with the underlying structure if the diffraction spots of the structure are all found on the Bragg diffraction spots of the superlattice. For a periodic system this definition is clear. A 2×2 commensurate superlattice has additional Bragg spots halfway between the original lattice spots, but also contains the original spots. For the dense set of diffraction spots from a quasicrystal it is not as obvious. Consider a one-dimensional case: the Fibonacci sequence. The diffraction spots occur at $(2\pi/a)(n+m\tau)$. Deflation of the sequence (grouping a "long" and a "short" to form a "superlong", and making a "supershort" from a "long") produces another Fibonacci sequence with all lengths increased by τ. The new diffraction spots occur at

$$(2\pi/\tau a)(n+m\tau)=(2\pi/a)(1-\tau)(n+m\tau)$$
$$=(2\pi/a)(n'+m'\tau)\ ,$$

which results from the fact that τ is a quadratic irrational (i.e., $\tau^2=\tau+1$). For quadratic irrationals

$$(n''+m''\tau)(n'+m'\tau)=n+m\tau\ .$$

Thus a deflation of the Fibonacci sequence has diffraction spots which occur at precisely the same position as the original sequence, and would correspond to a commensurate structure from our definition. Similarly, any arrangement which changed the positions of the Bragg spots by $(n'+m'\tau)$ would yield the same positions as the original set. (Note that all deflations are commensurate, but not all commensurate structures are simple deflations; while all numbers m/τ^n can be written as $n'+m'\tau$ not all $n'+m'\tau$ can be written as m/τ^n.) For the periodic pattern some of the commensurate flux lattices are known theoretically,[8,14] and the above definition applies. What we need to know now in order to verify the above definition is where the vortices sit on the quasicrystalline network.

ACKNOWLEDGMENTS

This work was supported at the University of Pennsylvania by the National Science Foundation through Grants No. DMR-83-18060 and DMR-85-19059 at the Laboratory for Research on the Structure of Matter. Part of this work was performed at the National Research and Resource Facility for Submicron Structures, which is supported by the National Science Foundation.

[1]R. D. Parks and W. A. Little, Phys. Rev. **133**, A97 (1964).
[2]B. Pannetier, J. Chaussy, R. Rammal, and J. C. Villegier, Phys. Rev. Lett. **53**, 1845 (1984); B. Pannetier, J. Chaussy, and R. Rammal, J. Phys. (Paris) Lett. **44**, L853 (1983).
[3]Dov Levine and Paul J. Steinhardt, Phys. Rev. Lett. **53**, 2477 (1984); D. Levine and P. J. Steinhardt, Phys. Rev. B **34**, 596 (1986).
[4]P. G. de Gennes, C. R. Acad. Sci. Ser. B **292**, 279 (1981); **292**, 9 (1981).
[5]S. Alexander, Phys. Rev. B **27**, 1541 (1983).
[6]R. Rammal, T. C. Lubensky, and G. Toulouse, Phys. Rev. B **27**, 2820 (1983).
[7]H. J. Fink, A. Lopez, and R. Maynard, Phys. Rev. B **26**, 5237 (1982); J. Simonin, D. Rodrigues, and A. Lopez, Phys. Rev. Lett. **49**, 944 (1982).
[8]S. Teitel and C. Jayaprakash, Phys. Rev. Lett. **51**, 1999 (1983).
[9]D. Stroud and W. Y. Shih, Mater. Sci. Forum **4**, 177 (1985).
[10]S. Hendricks and E. Teller, J. Chem. Phys. **10**, 147 (1942), P. W. Stephens and A. I. Goldman, Phys. Rev. Lett. **56**, 1168 (1986).
[11]G. Grest, P. M. Chaikin, and D. Levine (unpublished).
[12]A. Behrooz, M. J. Burns, H. Deckmann, D. Levine, B. Whitehead, and P. M. Chaikin, Phys. Rev. Lett. **57**, 368 (1986).
[13]Franco Nori, Qian Niu, Eduardo Fradkin, and Shau-Jin Chang (unpublished).
[14]T. C. Halsey, Phys. Rev. B **31**, 5728 (1985).